Applied Catalysis B: Environmental 278 (2020) 119347

Contents lists available at ScienceDirect

Applied Catalysis B: Environmental

journal homepage: www.elsevier.com/locate/apcatb

Mechanistic study of Fe(III) chelate reduction in a neutral electro-Fenton process

Xiao-Cheng Liu[a,1], Chuan-Shu He[a,1], Zi-Yang Shen[a], Wen-Qiang Li[a], Ning Chen[b], Jun-Sheng Song[a], Xiao-Guo Zhou[b], Yang Mu[a,*]

[a] CAS Key Laboratory of Urban Pollutant Conversion, Department of Applied Chemistry, University of Science & Technology of China, Hefei 230026, China
[b] Department of Chemical Physics, University of Science and Technology of China, Hefei 230026, China

ARTICLE INFO

Keywords:
Electro-Fenton
Fe(III) chelate reduction
Electron
Atomic H*
DFT calculations

ABSTRACT

Fe(III) chelate reduction is of great importance in the homogeneous neutral electro-Fenton (EF) process, but its reduction mechanisms with different reductive species remain unclear. In this study, the reduction mechanisms of several typical Fe(III) chelates through electron and atomic H* were investigated using experiments and density functional theory calculations. The results indicated that the electron reduction efficiencies for [Fe(III)-EDTA]$^-$ and [Fe(III)-EDDS]$^-$ chelates were 16.23 and 8.31 times higher compared to $[Fe(H_2O)_6]^{3+}$, which was featured by low $E_{LUMO-HOMO}$ and concentrated LUMO distribution around Fe atom. In contrast, the atomic H* reduction efficiency for $[Fe(III)\text{-}HA]^{3+}$ chelate was 10 times higher than that of electron, attributed to high chelation ability of HA and negative energy barrier of $[Fe(III)\text{-}HA]^{3+}$ reduction in the atomic H*-dominated system. Additionally, phthalocyanine (Pc) had insignificant effect on pollutant degradation efficiency in the neutral EF systems due to the lower chelate ability of Pc with Fe(III) compared to H_2O.

1. Introduction

The electro-Fenton (EF) process is efficient for degrading biorecalcitrant wastewater, but technical challenges remain at neutral pH [1]. Particularly, in the homogeneous EF process, the generation of solid $Fe(OH)_3$ is not favorable for iron cycling at neutral pH, inhibiting the production of hydroxyl radicals (·OH) in the Fenton reaction [2]. Therefore, various ligands are usually added to the homogeneous EF system to promote the solubility of iron complexes by generating chelate species under neutral conditions [3–5]. The behaviors of organic chelate species in EF process are always complicated at neutral pH, including reduction, oxidation, chelating competition, destruction, and precipitation reaction.

Iron chelates are of great importance in the neutral EF process because the degradation efficiency can be improved by chelates via accelerating the cycling of Fe(II)/Fe(III) [6]. The chelation of Fe(III) with ethylenediaminetetraacetic acid (EDTA) has been widely adopted to form soluble complexes, thereby accelerating the electron transfer between iron species [3]. Ethylenediamine-*N,N'*-disuccinic acid (EDDS) was also used to form a Fe(III)-EDDS complex to catalyze the EF process [7]. Additionally, Fe(II) phthalocyanine (FePc) has been used as a chelate to create a heterogeneous Fenton catalyst [8], and achieve continuous iron cycling and efficient degradation. Humic acids (HAs), which are widespread, are also efficient ligands of Fe(III) [9]. However, the presence of HA resulted in unexpected low pollutant removal efficiency in the EF process with a conventional carbon felt (CF) cathode, indicating potential limitations of iron cycling under these conditions [10]. Since various ligands have different impacts on the redox of Fe(II)/Fe(III), the ligands for the neutral EF process should be carefully selected.

Electrons from the cathode are generally considered active species for the reduction of Fe(III)-complexes to Fe(II)-complexes [1]. Specifically, the electron reduction process is that the Fe(III) species directly react with electrons from the cathode to generate Fe(II) species. The electron reduction pathway of Fe(III) chelate was found to be associated with the structural property of the chelate, such as orbital hybridization [11], the spin state of metal ions [12,13], and the functional groups of ligands [14]. Interestingly, the cathode-introduced atomic H* might be an alternative to facilitate the regeneration of the Fe(II)-complex when electron reduction pathway was inefficient, thus enhancing pollutant degradation [10]. As for atomic H* reduction process, H_2O is reduced by electrons from the cathode to form atomic H*, which would then

* Corresponding author.
E-mail address: yangmu@ustc.edu.cn (Y. Mu).
[1] These authors contributed equally to this work.

https://doi.org/10.1016/j.apcatb.2020.119347
Received 19 February 2020; Received in revised form 19 June 2020; Accepted 16 July 2020
Available online 17 July 2020
0926-3373/

reduce the Fe(III) species to produce Fe(II) species and H_2O. In order to produce more atomic H*, the cathode needs to be modified to facilitate the H_2O dissociation and enhance atomic H* adsorption.

Our previous study found that the Ni-deposited CF (Ni-CF) cathode could introduce enough atomic H* for the reduction of low electron activity of Fe(III) species, such as Fe(III)-HA [10]. The reasons for enhanced atomic H* generation for the Ni-CF cathode were explained by d-band center theory and convincing electrochemical characterization. Specifically, the results demonstrated that the Fe(III)-CIP and Fe(III)-HA could be more readily reduced by electron and atomic H*, leading to favorable pollutant degradation rate in electron- and atomic H*-dominated EF systems, respectively [10]. It raises an interesting issue that the type of chelates and the dominated reductive species may need to be considered simultaneously in order to promote the degradation efficiency in EF systems. Nevertheless, there have been no detailed experimental and theoretical investigations on the influences of the inherent properties of chelates on the reduction priority of atomic H* and electrons during the EF process. With respect to experimental strategies, the chelation efficiency, structure, and redox capacity of iron chelates could be examined using electron spin resonance (ESR) [15], Raman spectroscopy [16], and electrochemical characterization, respectively [6,10]. The density functional theory (DFT) calculation could be used to determine the highest occupied molecular orbital (HOMO) and lowest unoccupied molecular orbital (LUMO) to indicate the electrophilic capacity of metal chelates [17,18]. Furthermore, the feasibility of the reactions between iron chelates and reductive species could be evaluated by assessing the thermodynamic properties and energy barrier [12].

Herein, four typical ligands, including EDTA, EDDS, Pc, and HA were used to clarify the relationship between the structure of Fe(III) chelates and the reduction priority of atomic H* and electrons during the neutral EF process. The selected four ligands not only have been widely applied in Fenton related processes [3,7,8,10], and but also have the definite chelate structures for computational construction [3,13], leading to significant and convincing conclusions. Ibuprofen (IBU) was used as the pollutant to exclude the reductive degradation caused by electrons or atomic H* [19]. The degradation of IBU in the presence of various ligands was initially investigated in the neutral EF system using CF and Ni-deposited CF (Ni-CF) cathodes as electron- and atomic H*-dominated systems, respectively [10]. Subsequently, the structures of various Fe(III) chelates were verified using ESR, DFT simulation, and Raman spectroscopy. The regeneration feasibility of various Fe(II) chelates was analyzed using thermodynamic calculations. Moreover, the reduction priority by electrons or atomic H* of different Fe(III) chelates was evaluated by molecular orbital (MO) analysis, energy barrier calculation, and cyclic voltammetry (CV) measurements.

2. Experimental

2.1. Electrochemical experiments

The EF experiments were conducted with 300 mL of a 0.2 mM IBU (> 98 %, Aladdin, China) solution in an undivided two-electrode cell with a constant current of 50 mA using DC power (WYK-303S, Shenzhen Nolepower Technology Co., China). The CF (Qingdao Baofeng Graphite Material Co., China; 2 cm × 5 cm × 0.5 cm) cathode was modified using a Ni-deposit method to introduce atomic H*, as described in our recent work [10], where the Ni-CF cathode was also etched by HCl for 10 min to exclude H_2O_2 production from Ni°. In addition to the CF or Ni-CF cathode, a RuO_2-IrO_2-coated dimensionally stable anode (DSA) from Baoji Ruicheng Titanium Co. (China) was used. A solution containing 0.05 M Na_2SO_4, 0.2 mM Fe^{2+}, IBU, and the ligand was stirred for 1 h to complete the chelation process after pH adjustment to 7.0 with 0.1 M NaOH or H_2SO_4; the pH was monitored with a Hanna HI9025 pH meter. EDTA (0.2 mM) (> 98 %, Aladdin, China), 0.2 mM EDDS (> 98 %, Micxy, China), 0.2 mM Pc (> 98 %, Aladdin, China), or 0.4 mM HA (> 90 %, Aladdin, China) was used to create a six-coordinated chelate complex [20]. The solution was subsequently bubbled for 30 min with compressed air at a rate of 0.4 L/min before electrolysis. In order to evaluate the Fe(III) reduction with H_2O_2, additional H_2O_2 (30 % w/w, Merck, USA) was added into the EF system before experiments. All other chemicals were of analytical grade and were obtained from Sigma-Aldrich (USA), and the HA was purified three times as outlined previously [21].

The IBU degradation was followed by high-performance liquid chromatography (HPLC) (Agilent, USA) analysis using an Eclipse Plus C18 column (0.46 × 25 cm, 5-μm particle size). The mobile phase for the determination of the IBU was a 0.25 M acetic acid/acetonitrile (25:75, v/v) mixture at a flow rate of 0.5 mL/min, and the wavelength was 221 nm [22]. The removal rate constant (k_{obs}) was obtained from the pseudo-first-order fitting of the degradation of IBU during the reaction time. The Fe(II) concentration in the presence of different ligands was measured using a 1,10-phenanthroline colorimetric method [7]. The concentration of the dissolved iron was determined using inductively coupled plasma-atomic emission spectrometry (ICP-AES, PerkinElmer, USA). A Bruker 200A-9.5 ESR spectrometer (JEOL, Japan) was used to detect the signal of the Fe(III) chelates at neutral pH [15]. The details of the electrochemical characterization of the chelate species are provided in the Supporting Information (Texts SI-1).

2.2. Raman spectra measurements

The Raman spectrometer data of the Fe(III) chelates were obtained as described in our recent work [23,24]. Briefly, the excitation source was a CW laser (Coherent, Verdi) at 532 nm with a power of 2 W. A triple-monochromator system (Acton Research, TriplePro) was used to disperse the Raman scattered light. The dispersed spectra were recorded at a resolution of ca. 1 cm^{-1} by a liquid nitrogen-cooled CCD detector (Princeton Instruments, Spec-10:100B) in the region of $300-700$ and $1280-1680\ cm^{-1}$. The Raman shift was calibrated using a mercury lamp, and a quartz cuvette was used to store the sample solution. The acquisition time was ca. 20 s for each measurement, and 30 measurements of the Raman spectra of each chelate were averaged.

2.3. DFT calculations

The DFT calculations of the iron chelates and related ligand molecules were performed in the DMol^3 module, including the simulated Raman spectra, thermodynamic properties, MO distribution, and energy barrier (E_a). All of the iron chelate structures were optimized by the Perdew-Wang 91 (PW91) generalized gradient approximation (GGA) using an all-electron method. The exchange-correlation term, conductor-like screening model (COSMO), and double-precision numerical basis sets with polarization functions (DNP) were adopted [25]. The convergence threshold of each geometry optimization cycle was 1×10^{-5} Hartree, and the maximum tolerances of the force and displacement were 2×10^{-3} Hartree/Å and 5×10^{-3} Å, respectively. The E_a and transition state (TS) were determined using the linear synchronous transit (LST)/quadratic synchronous transit (QST) methods [26]. The free energy difference (ΔG) is defined in Eq. (1) [27].

$$\Delta G = \Delta H - T\Delta S = \Delta E + \Delta\ \mathrm{ZPVE} + \int_0^T \Delta C_p dT - T\Delta S = \Delta E + \Delta H_{corr} - T\Delta S \quad (1)$$

where ΔG, ΔH, ΔE, ΔZPVE, ΔC_p, ΔS, and ΔH_{corr} are the changes in the free energy, enthalpy, total energy, zero-point energies, heat capacity, entropy, and temperature-corrected enthalpy. The values of ΔE, ΔS, and ΔH_{corr} were obtained from the DFT calculations.

2.4. Computational models

The iron atom was six-coordinated with the ligands (L) $EDTA^{4-}$, $EDDS^{4-}$, Pc^{2-}, HA, and H_2O to establish the common octahedral configuration [20]. The $[Fe(II)\text{-}EDTA]^{2-}$, [Fe(III)-EDTA]-, $[Fe(II)\text{-}EDDS]^{2-}$, [Fe(III)-EDDS]-, $[Fe(II)\text{-}Pc]\cdot 2H_2O$, and $[Fe(III)\text{-}Pc]^{+}\cdot 2H_2O$ complexes were created at an L:Fe(III) molar ratio of 1:1 [12]; two H_2O molecules were introduced to create the FePc structure with an octahedral configuration [13,28]. Specifically, the $[Fe(II)\text{-}HA]^{2+}$ and $[Fe(III)\text{-}HA]^{3+}$ complexes were created at an L:Fe(III) molar ratio of 1:2 because the HA used in this study has 3 coordinated sites. The $[Fe(H_2O)_6]^{3+}$ and $[Fe(H_2O)_6]^{2+}$ complexes were created at an L:Fe(III) molar ratio of 1:6 [29]. Additionally, all Fe(III) chelates had a high-spin state, whereas the Fe(II) chelates had a low-spin state [30]. The optimized structure of Ni-CF was introduced to TS search of the Fe(III) chelate reduction, providing an adsorption site for the atomic H*. The water molecule was introduced to accept H^+, resulting in the generation of a hydrated proton after the reduction of the Fe(III) chelate.

3. Results and discussion

3.1. Effects of various chelates on IBU removal

The removal of IBU was conducted at an initial neutral pH, and the CF and Ni-CF cathodes represented the electron- and atomic H*-dominated EF systems, respectively. The variations of solution pH were checked in the EF process with the CF cathode in the presence of different ligands, as shown in Fig. SI-1. The solution pH changed slightly in the presence of EDTA, EDDS, and HA, while only decreased from 7.0 to 5.8 without the addition of the ligand and in the presence of Pc. Indeed, the H* based processes could generate protons after the reduction of Fe(III), but the generation of H* would also consume protons from the H_2O, resulting in an insignificant impact on pH variation. In the EF system, the reduction of pH was mainly caused by hydrolysis of Fe(III) in the absence of efficient chelating agent [10]. However, the EDTA, EDDS, and HA can effectively chelate with Fe(III) and thus prevent the hydrolysis of Fe(III), inhibiting the decrease in the solution pH. The interfacial pH variation may be different for modified and unmodified cathodes [31], which could influence the reduction of iron chelates on the cathode and thus need a further investigation.

Fig. 1a shows that the degradation rate constant of IBU for Ni-CF ($0.0047\ min^{-1}$) was higher than that of CF ($0.0013\ min^{-1}$) in the absence of additional ligand, confirming that the presence of atomic H* promoted the reduction of the Fe(III)-H_2O complex; the reason was that the Fe(III)-IBU chelate had negligible electro-activity [22,32]. It should be noted that H_2O_2 accumulation for the Ni-CF cathode was found to be slightly lower than that of the CF cathode [10], suggesting that Ni-CF and pristine CF exhibited the comparable electrocatalytic activity for H_2O_2 production. Therefore, the difference in ibuprofen degradation efficiency in the electro-Fenton process would likely result from different Fe(III) reduction efficiency of various cathodes.

As shown in Fig. 1b, the IBU degradation rate constant was 16.23 and 8.31 times higher in the EF system with the CF cathode after the addition of EDTA and EDDS, respectively. This result was attributed to the more easily chelation efficiency of the EDTA and EDDS with Fe(III) than with H_2O [3]. Interestingly, the addition of EDTA and EDDS only resulted in 2.29 and 2.61 times higher IBU degradation rate constants in the atomic H*-dominated EF system (Fig. 1b). The electron-dominated system was much more favorable to reduce the Fe(III)-EDTA and Fe (III)-EDDS complexes than the atomic H*-dominated system. In addition, the Fe(III)-EDTA complex was more readily reduced than the Fe (III)-EDDS complex by the electron-dominated system. The Pc addition had no significant effect on the IBU degradation in the electron- and atomic H*-dominated EF systems (Fig. 1b). Interestingly, the rate constant of the IBU degradation in the presence of HA was one half of that in the absence of HA in the electron-dominated EF system (Fig. 1b).

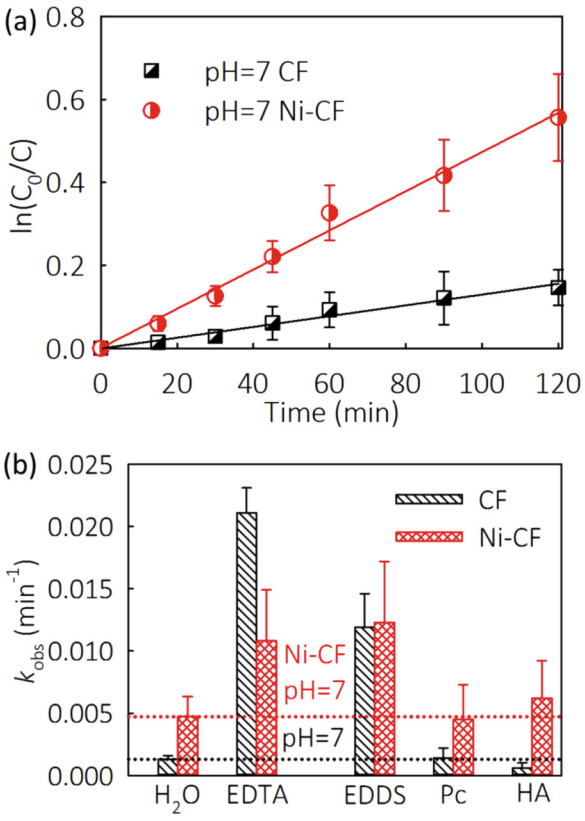

Fig. 1. (a) IBU degradation in two EF systems (0.2 mM IBU at a current of 50 mA, 0.05 M Na_2SO_4, 0.2 mM Fe^{2+}, and pH = 7.0). (b) Effects of EDTA, EDDS, Pc, and HA on the degradation rate constant of IBU in two EF systems (0.2 mM IBU at a current of 50 mA, 0.05 M Na_2SO_4, 0.2 mM Fe^{2+}, initial pH = 7.0, and 0.2 mM EDTA, 0.2 mM EDDS, 0.2 mM Pc, 0.4 mM HA, respectively).

However, the IBU degradation rate constant in the atomic H*-dominated EF system was 10.33 times higher than that in the electron-dominated EF system in the presence of HA (Fig. 1b), implying that atomic H* enhanced the reduction of the Fe(III)-HA chelate.

The variations of the Fe(II) concentration were determined in different systems, as shown in Fig. SI-2. The addition of EDDS increased the available Fe(II) concentration at neutral pH as compared to the addition of Pc, HA as well as without the ligand [7]. The atomic H*-dominated reduction system increased the concentration of Fe(II) in the presence of HA as compared to electron-dominated reduction system, which was even higher than that of Pc and without the addition of the ligand. Moreover, the concentration of Fe(II) was higher in the atomic H*-dominated system compared to the electron-dominated on at the presence of HA. Unfortunately, the available Fe(II) with the EDTA addition could not be accurately detected due to the greater formation constants of Fe(II) chelate with EDTA than 1,10-phenanthroline [33]. Nonetheless, it can be deducted that the actual Fe(II) concentration in the presence of EDTA would be comparable with that in the presence of EDDS due to similar pollutant degradation performance.

The effects of chelate and Fe(III) concentrations, electrolyte concentration, and initial pH on the performance of two EF systems were explored in the presence of EDTA and HA. In order to ensure that the iron atom is six-coordinated with the ligand, the EDTA and HA were added at an L:Fe(II) molar ratio of 1:1 and 1:2 during investigating the effects of chelate and Fe(III) concentrations, respectively. As shown in Fig. SI-3a, the best degradation of IBU was achieved with addition of 0.2 mM Fe(II) and 0.2 mM EDTA, and 0.4 mM Fe(II) and 0.8 mM HA in both EF systems, respectively. The decay rate constant of IBU was comparable with 0.025 and 0.05 mM Na_2SO_4 in two EF systems, while

it reduced in the presence of 0.1 M Na_2SO_4 (Fig. SI-3b). The inhabitation of IBU removal in 0.1 M Na_2SO_4 might be caused by the transformation from ·OH into less efficient $SO_4^{\cdot -}$ in the presence of excess SO_4^{2-} [34]. As shown in Fig. SI-3c, the acidic pH generally accelerated the degradation of IBU in two EF systems. However, initial pH had a more significant impact on IBU degradation in the presence of HA compared to EDTA. It was previously reported that the variation of initial pH from 5.0 to 9.0 made little difference to the ratio of soluble Fe (III) in the presence of EDTA [2], which may explain unobvious change of IBU removal in EDTA chelation EF system (Fig. SI-3c). Conversely, the acidic pH could cause the dissociation of Fe(III)-HA into Fe(III) and HA [35], which may particularly lead to a 8.67-time higher IBU decay rate constant than that at neutral pH in electron-dominated EF systems (Fig. SI-3c).

Furthermore, the NaCl was employed as the electrolyte to investigate the impact of excess chloride on IBU degradation in two EF systems in the presence of EDTA and HA. As shown in Fig. SI-3d, the degradation rate constant of IBU with 0.05 M NaCl is lower than that with 0.05 M Na_2SO_4 in all of systems, suggesting that the excess chloride had a negative impact on IBU removal in EF systems. This could be explained by the scavenger effect of Cl^- on hydroxyl radical, producing less powerful active chlorine species, such as $ClOH^{\cdot -}$ and $Cl^{\cdot}$ [34,36]. As for the chelation aspects, the competition of chloride with organic chelates can be ignorable due to the low formation constant of Fe(III)-chloride [34]. Meanwhile, the competition of bicarbonate was not considered in this study, due to the acute hydrolysis in the coexistence of Fe^{3+} and CO_3^{2-} [37].

3.2. Structure identification of different Fe(III) chelates

The ESR signal of Fe(III) (Fig. 2) indicates the generation of stable chelates with EDTA, EDDS, or HA, as well as the lower chelation efficiency of Pc than H_2O. The higher intensity of ESR spectra means more soluble Fe(III) species in aqueous solution [15], suggesting that the ligand has a better chelation efficiency to dissolve more $Fe(OH)_3$ into soluble Fe(III) compared to water under neutral pHs [2]. In this study, if the intensity of ESR spectra of Fe(III) chelate is higher that of $[Fe(H_2O)_6]^{3+}$, this Fe(III) chelate is defined as the high chelate, such as Fe (III)-EDTA, Fe(III)-EDDS and Fe(III)-HA.

The structures of various iron chelates were proposed and optimized in the calculation package DMol^3, including $[Fe(II)\text{-}EDTA]^{2-}$, [Fe(III)-EDTA]-, $[Fe(II)\text{-}EDDS]^{2-}$, [Fe(III)-EDDS]-, $[Fe(II)\text{-}Pc]\cdot 2H_2O$, $[Fe(III)\text{-}Pc]^{+}\cdot 2H_2O$, $[Fe(II)\text{-}HA]^{2+}$, and $[Fe(III)\text{-}HA]^{3+}$. Subsequently, the Raman spectra of the corresponding Fe(III) chelates were calculated

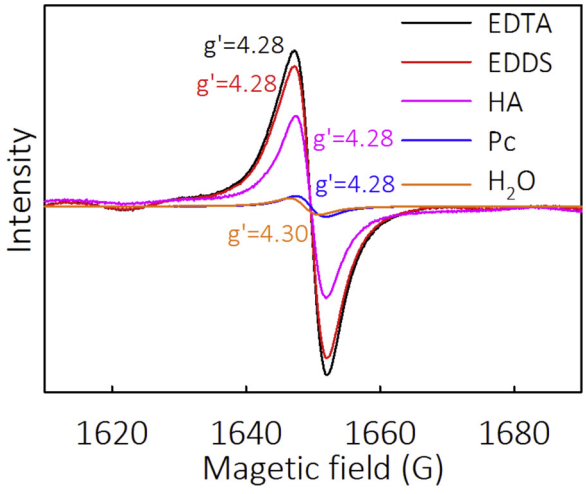

Fig. 2. ESR spectra of the Fe(III) signal region for the chelate of [Fe(III)-EDTA]$^-$, [Fe(III)-EDDS]$^-$, $[Fe(III)\text{-}Pc]^{+}\cdot 2H_2O$, $[Fe(III)\text{-}HA]^{3+}$, and $[Fe(H_2O)_6]^{3+}$ at neutral pH.

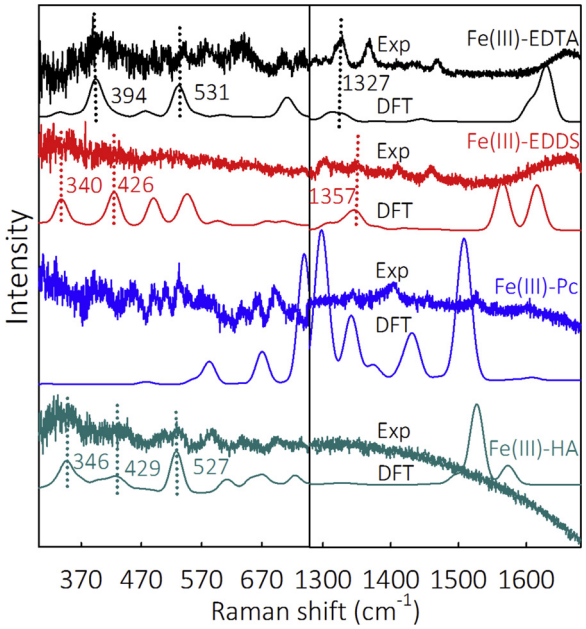

Fig. 3. Observed and calculated Raman spectra of various Fe(III) chelates.

based on the optimized structure. As shown in Fig. 3, the Raman scattering in the region of 300 − 700 cm^{-1} represents the vibration between the Fe atom and the O or N atom [16], covering the peaks at 394 and 531 cm^{-1} of [Fe(III)-EDTA]-, the peaks at 340 and 426 cm^{-1} of [Fe(III)-EDDS]-, and the peaks at 346, 429, and 527 cm^{-1} of $[Fe(III)\text{-}HA]^{3+}$ (Fig. 3). In addition, the peaks of [Fe(III)-EDTA]- and [Fe(III)-EDDS]-centered at 1327 and 1357 cm^{-1} were assigned to the carbon-based functional group [16]. Raman measurements were obtained to identify Fe(III) chelates in aqueous solution [38], where $Fe_2(SO_4)_3$ was used to fabricate [Fe(III)-EDTA]-, [Fe(III)-EDDS]-, $[Fe(III)\text{-}Pc]^{+}\cdot 2H_2O$, and $[Fe(III)\text{-}HA]^{3+}$ to avoid oxidation of Fe(II) during the Raman measurements. As indicated in Fig. 3, the experimental data were well consistent with the simulated results for [Fe(III)-EDTA]-, [Fe(III)-EDDS]-, and $[Fe(III)\text{-}HA]^{3+}$, and the three peaks of the Raman spectra of each chelate exhibited good matches [38]. In the 1280 − 1680 cm^{-1} region, the peak indicating the functional group of $[Fe(III)\text{-}HA]^{3+}$ was greatly suppressed by the fluorescence even after several hours of quenching (Fig. 3), although several peaks were found in the calculated Raman spectrum. Nevertheless, there was a poor agreement between the simulated and measured Raman spectra for $[Fe(III)\text{-}Pc]^{+}\cdot 2H_2O$, indicating that $[Fe(III)\text{-}Pc]^{+}\cdot 2H_2O$ might not be the dominant chelate species in the mixture of Pc and Fe(III), as shown in the ESR spectra (Fig. 2). The identified structures of the different Fe(III) chelates were used in the following DFT calculations.

3.3. Thermodynamic aspect of Fe(II) chelate regeneration

Generally, the substitution of $[Fe(H_2O)_6]^{2+}$ and reduction of Fe(III) chelate are two direct approaches to generate the Fe(II) chelate. The substitution of $[Fe(H_2O)_6]^{2+}$ was conducted by using a specific ligand, and the formation energy (ΔG_f) from $[Fe(H_2O)_6]^{2+}$ to the Fe(II) chelate was calculated using the following equations:

$$\Delta G_f([Fe(II)\text{–}EDTA]^{2-}) = G([Fe(II)\text{–}EDTA]^{2-}) + 6\,G(H_2O) - G([Fe(H_2O)_6]^{2+}) - G(EDTA^{4-}) \quad (2)$$

$$\Delta G_f([Fe(II)\text{–}EDDS]^{2-}) = G([Fe(II)\text{–}EDDS]^{2-}) + 6\,G(H_2O) - G([Fe(H_2O)_6]^{2+}) - G(EDDS^{4-}) \quad (3)$$

$$\Delta G_f([\mathrm{Fe(II)-Pc}]\cdot 2H_2O) = G([\mathrm{Fe(II)-Pc}]\cdot 2H_2O) + 4\,G(H_2O) - G([\mathrm{Fe}(H_2O)_6]^{2+}) - G(\mathrm{Pc}^{2-}) \quad (4)$$

$$\Delta G_f([\mathrm{Fe(II)-HA}]^{2+}) = G([\mathrm{Fe(II)-HA}]^{2+}) + 6\,G(H_2O) - G([\mathrm{Fe}(H_2O)_6]^{2+}) - 2G(\mathrm{HA}) \quad (5)$$

The calculation of ΔG_f is applicable to both the electron- and atomic H*-dominated EF systems, but the Gibb's energy change (ΔG) of the electron reduction of the Fe(III) chelates could not be directly calculated because the energy of a single electron is not accessible. Herein, the proton-coupled reduction reaction was used to describe the atomic H*-dominated reduction process (Eq. (6)) [39]. Since the Gibb's energy of the free atomic H* is equal to half of H_2 (Eq. (7)) [40], the ΔG for the reduction of Fe(III) with a specific ligand (L) is calculated using Eq. (8).

$$\mathrm{Fe(III)-L\,(solv) + H_2O(aq) + H^*(aq) \rightarrow Fe(II)-L(solv) + H_3O^+(aq)} \quad (6)$$

$$G(\mathrm{H^*}) = \frac{1}{2}G(H_2) \quad (7)$$

$$\Delta G(\mathrm{Fe(III)/Fe(II)}) = G(\mathrm{Fe(II)-L}) + G(H_3O^+) - \frac{1}{2}G(H_2) - G(\mathrm{Fe(III)-L}) - G(H_2O) \quad (8)$$

All the thermodynamic calculations were calibrated to standard conditions at 298.15 K; the free energy changes for the chelate and ligand species are given in Table SI-1. Consequently, the formation energies of $[\mathrm{Fe(II)\text{-}EDTA}]^{2-}$, $[\mathrm{Fe(II)\text{-}EDDS}]^{2-}$, $[\mathrm{Fe(II)\text{-}Pc}]\cdot 2H_2O$, and $[\mathrm{Fe(II)\text{-}HA}]^{2+}$ from $[\mathrm{Fe}(H_2O)_6]^{2+}$ were estimated at -5.7, -6.3, 9.5, and -1.0 eV, respectively (Fig. 4). Except for $[\mathrm{Fe(II)\text{-}Pc}]\cdot 2H_2O$, the transformations from $[\mathrm{Fe}(H_2O)_6]^{2+}$ to $[\mathrm{Fe(II)\text{-}EDTA}]^{2-}$, $[\mathrm{Fe(II)\text{-}EDDS}]^{2-}$, and $[\mathrm{Fe(II)\text{-}HA}]^{2+}$ are spontaneous, indicating their high chelate feature [41]. This result could be validated with the ESR analysis, in which the intensity of ESR spectra increased after adding EDTA, EDDS and HA (Fig. 2). As illustrated in Fig. 4, the thermodynamic energy profile of the atomic H*-dominated reduction of the Fe(III)-chelates was significantly affected by the type of ligands, and the Gibb's energy changes for H_2O, EDTA, EDDS, Pc, and HA were -2.1, 1.8, 1.6, 17.1, and -0.1 eV, respectively. Interestingly, only the reductions of $[\mathrm{Fe}(H_2O)_6]^{3+}$ and $[\mathrm{Fe(III)\text{-}HA}]^{3+}$ in the atomic H*-dominated system are spontaneous, whereas the atomic H*-dominated pathway does not appear to be favorable for the reduction of [Fe(III)-EDTA]-, [Fe(III)-EDDS]-, and $[\mathrm{Fe(III)\text{-}Pc}]^{+}\cdot 2H_2O$.

3.4. Reduction priority of electrons with Fe(III) chelates

The reduction priority of electrons was evaluated by conducting qualitative and quantitative analyses of HOMO and LUMO, revealing the electrophilic site and k_{obs}–related energy profile of the chelate species [18,42,43]. The LUMOs of $[\mathrm{Fe(III)\text{-}EDTA}]^{-}$ and $[\mathrm{Fe(III)\text{-}EDDS}]^{-}$ are more concentrated near the Fe atom than those of the $[\mathrm{Fe(III)\text{-}Pc}]^{+}\cdot 2H_2O$ and $[\mathrm{Fe(III)\text{-}HA}]^{3+}$ (Fig. 5), indicating that the Fe(III) sites for the $[\mathrm{Fe(III)\text{-}EDTA}]^{-}$ and $[\mathrm{Fe(III)\text{-}EDDS}]^{-}$ are more favorable to accept electrons [18]. The LUMOs of $[\mathrm{Fe(III)\text{-}Pc}]^{+}\cdot 2H_2O$ and $[\mathrm{Fe(III)\text{-}HA}]^{3+}$ occur primarily on the Pc and HA ligands (Fig. 5), indicating that Pc or HA is more readily reduced by electrons than the Fe center. Interestingly, the HOMOs of $[\mathrm{Fe}(H_2O)_6]^{3+}$ and $[\mathrm{Fe}(H_2O)_6]^{2+}$ exhibit broad overlap with the LUMOs around the Fe atom (Fig. 5), suggesting that electron reduction occurs less readily in $[\mathrm{Fe}(H_2O)_6]^{3+}$ [44].

The qualitative analysis of the electron affinity of each Fe(III) chelate was identified using CV measurements with the CF cathode, as shown in the SI [6]. A reduction in the peak of the CV curves was only found in the presence of EDTA or EDDS at neutral pH (Fig. 6), indicating that the reduction of Fe(III)-EDTA and Fe(III)-EDDS chelates is favorable on the CF cathode, which is in agreement with the concentrated LUMO distribution around the Fe atom (Fig. 5). Additionally, the absence of a redox peak in the complexes without Pc, HA or chelate suggests unfavorable electron reduction of the related iron chelates; this result is in line with the distribution of LUMOs on the ligand.

The E_{LUMO} and E_{HOMO} were calculated to obtain quantitative measurements to clarify the reduction of the Fe(III) chelates (Table SI-2). The E_{LUMO} shows the capacity of Fe(III) chelate to accept electrons, whereas the $E_{LUMO\text{-}HOMO}$ represents the energy gap for the activation of Fe(III) chelate [45]. The plot of E_{LUMO} vs. ln k_{obs} is illustrated in Fig. 7a; a weak linear correlation was found for $[\mathrm{Fe(III)\text{-}EDTA}]^{-}$, $[\mathrm{Fe(III)\text{-}EDDS}]^{-}$, and $[\mathrm{Fe(III)\text{-}Pc}]^{+}\cdot 2H_2O$. However, the E_{LUMO} values of $[\mathrm{Fe(III)\text{-}HA}]^{3+}$ and $[\mathrm{Fe}(H_2O)_6]^{3+}$ were not correlated with the ln k_{obs}; the reason might be than an increase in the number of ligands at the iron center contributed to a lower E_{LUMO} of the chelate species [46]. In order to construct a six-coordinated iron atom in the DFT calculation, the number of ligands was fixed for each Fe(III)-L complex, as the coordinate sites of each ligand is definite, such as 3 for HA and 1 for H_2O [29]. Hence, the impact of number of chelates on the redox capacity of Fe center among different chelates has been considered and compared in the DFT calculations. In contrast, as shown in Fig. 7b, a strong linear correlation between $E_{LUMO\text{-}HOMO}$ and ln k_{obs} was observed for the $[\mathrm{Fe(III)\text{-}EDTA}]^{-}$, $[\mathrm{Fe(III)\text{-}EDDS}]^{-}$, $[\mathrm{Fe(III)\text{-}HA}]^{3+}$, and $[\mathrm{Fe}(H_2O)_6]^{3+}$, implying that Fe(III) chelates with a lower $E_{LUMO\text{-}HOMO}$ might be more favorable for electron reduction. Fig. 7b also shows the $E_{LUMO\text{-}HOMO}$ for $[\mathrm{Fe(III)\text{-}HA}]^{3+}$ (1.88 eV) is higher than $[\mathrm{Fe}(H_2O)_6]^{3+}$ (1.70 eV), indicating that the electron reduction of $[\mathrm{Fe(III)\text{-}HA}]^{3+}$ is more difficult than that of $[\mathrm{Fe}(H_2O)_6]^{3+}$. This might explain half degradation rate constant of IBU after the addition of HA in the electron-dominated EF system compared to the atomic H*-dominated one (Fig. 1b). However, the $[\mathrm{Fe(III)\text{-}Pc}]^{+}\cdot 2H_2O$ fell outside the line, possibly because $[\mathrm{Fe}(H_2O)_6]^{3+}$ is the active Fe species under these conditions due to the low chelation efficiency of Pc (Fig. 2). In summary, the experimental and theoretical analyses suggest that the electron reduction pathway might be more favorable for $[\mathrm{Fe(III)\text{-}EDTA}]^{-}$ and $[\mathrm{Fe(III)\text{-}EDDS}]^{-}$ than for $[\mathrm{Fe(III)\text{-}Pc}]^{+}\cdot 2H_2O$, $[\mathrm{Fe(III)\text{-}HA}]^{3+}$, and $[\mathrm{Fe}(H_2O)_6]^{3+}$ in EF systems.

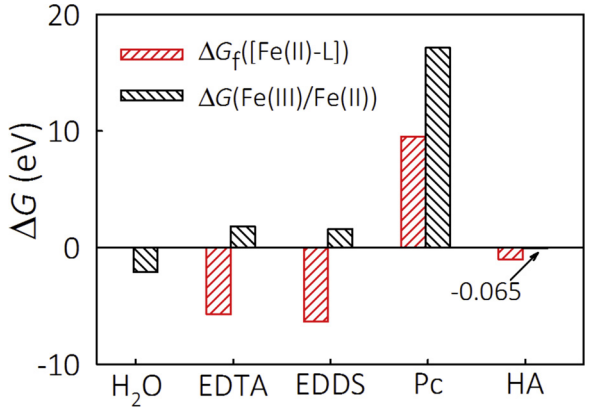

Fig. 4. Calculated formation energy of Fe(II)-L and standard Gibb's free energy changes in the atomic H* reduction of Fe(III)-L.

3.5. Reduction priority of atomic H* with Fe(III) chelates

The atomic H* generated by the Ni-CF cathode does not exist in aqueous solution as other radicals, and the d-band center of the surface of the electrode is suitable to stabilize the atomic H* [10]. As shown in Fig. 8, the optimized structure of the interaction configuration of the atomic H*-attached surface of the Ni-CF electrode is defined as the initial state, whereas the isolated one is the final state. This process stands for the electron transfer from atomic H* to the Fe(III) chelates. Fig. 9 shows that the energy barriers for the atomic H*-dominated reduction of the EDTA and EDDS chelates were 2.07 and 0.59 eV, respectively, implying that the atomic H* must overcome these energy barriers to reduce $[\mathrm{Fe(III)\text{-}EDTA}]^{-}$ and $[\mathrm{Fe(III)\text{-}EDDS}]^{-}$. This might be

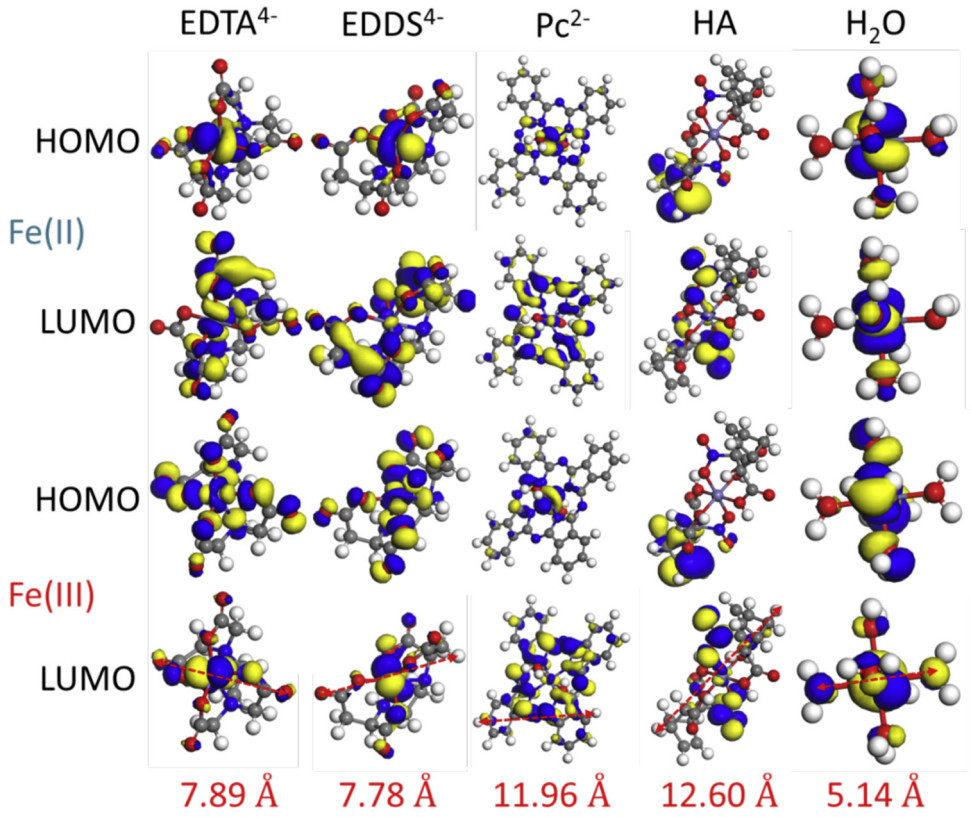

Fig. 5. HOMO and LUMO distributions of $[Fe(II)\text{-}EDTA]^{2-}$, [Fe(III)-EDTA]-, $[Fe(II)\text{-}EDDS]^{2-}$, [Fe(III)-EDDS]-, $[Fe(II)\text{-}Pc]\cdot 2H_2O$, $[Fe(III)\text{-}Pc]^{+}\cdot 2H_2O$, $[Fe(II)\text{-}HA]^{2+}$, $[Fe(III)\text{-}HA]^{3+}$, $[Fe(H_2O)_6]^{2+}$, and $[Fe(H_2O)_6]^{3+}$.

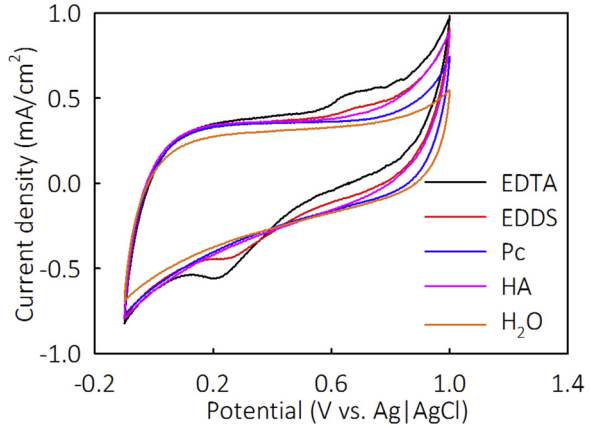

Fig. 6. CV curves in the presence of $[Fe(II)\text{-}EDTA]^{2-}$, $[Fe(II)\text{-}EDDS]^{2-}$, $[Fe(II)\text{-}Pc]\cdot 2H_2O$, $[Fe(II)\text{-}HA]^{2+}$, and $[Fe(H_2O)_6]^{2+}$ with CF at neutral pH.

the major reason that the addition of EDTA and EDDS only increased the degradation rate constant of IBU by 2.29 and 2.61 times in the atomic H*-dominated EF system (Fig. 1b). In contrast, the values of the energy barrier of the Fe(III) chelates of Pc, HA, and H_2O were in the negative ranges (Fig. 9), suggesting that the $[Fe(III)\text{-}Pc]^{+}\cdot 2H_2O$, $[Fe(III)\text{-}HA]^{3+}$, and $[Fe(H_2O)_6]^{3+}$ were reduced by atomic H* without an energy barrier [47].

Experimental identification of the atomic H* affinity for each chelate was performed using the CV measurements with the Ni-CF cathode. The presence of an oxidation peak of atomic H* in the EDTA and EDDS systems suggests unreacted atomic H* on the Ni-CF (Fig. 10), verifying the positive energy barrier values of these systems (Fig. 9). Interestingly, the stronger atomic H* peak quenching effect of EDDS implies that the Fe(IIII)-EDDS chelate had higher atomic H* affinity than EDTA, which corresponded to the lower energy barrier (Fig. 9) and less inhibition of IBU degradation in the atomic H*-dominated system (Fig. 1b). The complete quenching of the atomic H* peak in the presence of Pc and HA, as well as without chelate, is in agreement with the negative energy barriers for the reaction of these Fe(III) chelates with atomic H* (Fig. 9). In addition, these results also verified the spontaneous reduction of $[Fe(H_2O)_6]^{3+}$ and $[Fe(III)\text{-}HA]^{3+}$ in thermodynamic calculations (Fig. 4).

Interestingly, the $[Fe(III)\text{-}HA]^{3+}$ system was most favorable for the atomic H*-dominated EF system (Fig. 1b), although the energy barrier of the $[Fe(III)\text{-}HA]^{3+}$ reduction by atomic H* was 0.75 and 0.54 eV higher than that of $[Fe(III)\text{-}Pc]^{+}\cdot 2H_2O$ and $[Fe(H_2O)_6]^{3+}$ (Fig. 9). The chelation of HA with Fe(III) was more easily than that of Pc and H_2O according to the ESR spectra (Fig. 2). The high chelation efficiency of HA seems to play a vital role in the atomic H* reduction, contributing to stronger IBU degradation capacity compared to the systems with Pc and without additional chelates (Fig. 1b). The destruction of Fe(III) chelate could cause a poor electron reduction at neutral pH, which would not achieve high percentages of mineralization in EDTA and EDDS systems. Interestingly, our result suggests that the Ni-CF cathode could even promote pollutant degradation without addition of organic ligands, which is expected to achieve high percentages of mineralization [10]. Therefore, there would be of great significance in modifying carbon felt with Ni to work at neutral pH with complexed iron in EF systems. Indeed, the complicated water matrix may also contain many naturally-occurring organics and inorganics, which more readily react with electron than atomic H*. Under such conditions, there would be a competition between electron and atomic H* reduction in the EF system, making the whole process more complex. Therefore, it deserves a further investigation for the complicated water matrix particularly in the atomic H*-dominated EF system.

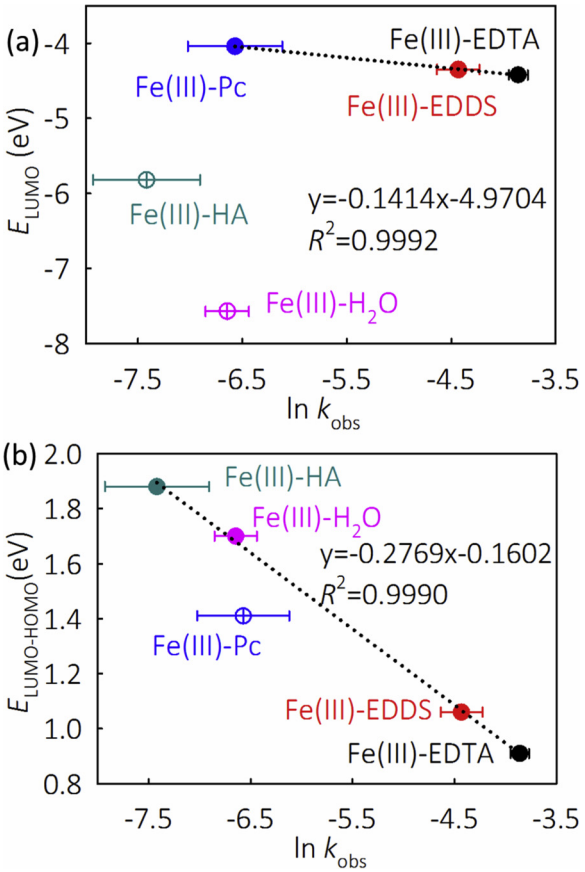

Fig. 7. Plots of (a) E_{LUMO} and (b) $E_{LUMO\text{-}HOMO}$ vs. ln k_{obs} of IBU degradation in the EF system with the CF cathode.

3.6. Reduction mechanism of Fe(III) in neutral EF process

As shown in Scheme 1, the cathode plays a critical role in the reduction of Fe(III) chelate in the neutral EF process. We have previously proved that the Fe(III) chelate could be effectively reduced by cathode-introduced atomic H* [10]. In this work, the ligand-dependent cathode reduction priority of electron and atomic H* was explored, which could be directly evaluated by LUMO distribution, $E_{LUMO\text{-}HOMO}$, and energy barrier calculation. Particularly, the transformation between the Fe(III)-L and $[Fe(H_2O)_6]^{3+}$ was taken into considered, and the reduction priority of atomic H* for $[Fe(H_2O)_6]^{3+}$ was identified. Additionally, it has been previously demonstrated that H_2O_2, $HO_2^{\cdot}/O_2^{\cdot-}$ and organic radicals ($R^{\cdot}$) could also conduct the reduction of Fe(III)-L and $[Fe(H_2O)_6]^{3+}$ in bulk solution [48–50], which would inspire homogeneous Fenton reaction to produce $^{\cdot}OH$.

In order to evaluate the possible contribution of Fe(III) reduction with H_2O_2 route, some experiments were further conducted. Firstly, as shown in Fig. S4, the addition of 30 mg/L H_2O_2 into the EF system further enhanced the degradation of IBU in the presence of EDTA and EDDS, but had slight impact on IBU degradation rate constant in the presence of Pc and HA. Secondly, the actual H_2O_2 concentration in the presence of EDTA (< 3 mg/L) with the CF cathode was lower than that of the Ni-CF cathode (< 6 mg/L) during first 1 h of EF process (data not provided). Considering that the degradation rate constant of IBU with Ni-CF (0.0108 min^{-1}) cathode was lower than that of CF (0.0211 min^{-1}) cathode (Fig. 1b) in the presence of EDTA, the relatively higher H_2O_2 concentration would not be sufficient to alter the major Fe(III) reduction routes. Therefore, it could be concluded that the contribution of H_2O_2 to Fe(III) reduction was relatively limited as compared to the favorable cathodic reduction pathway in this study.

On the other hand, indeed the $R^{\cdot}$ could be generated from the alkyl hydroxylation and may conduct the Fe(III) reduction [51]. However, it has been indicated that the Fe(III) reduction with $R^{\cdot}$ route is not efficient and some of $R^{\cdot}$ species even tend to facilitate Fe(II) oxidation rather than Fe(III) reduction [52]. In addition, unfortunately there are no standard methods to introduce or quantify $R^{\cdot}$ in each chelate system, and moreover the types of $R^{\cdot}$ might be not comparable in the presence of different organic chelates, making it difficult for quantitative analysis of $R^{\cdot}$ contribution on Fe(III) reduction. Although we think that the $R^{\cdot}$

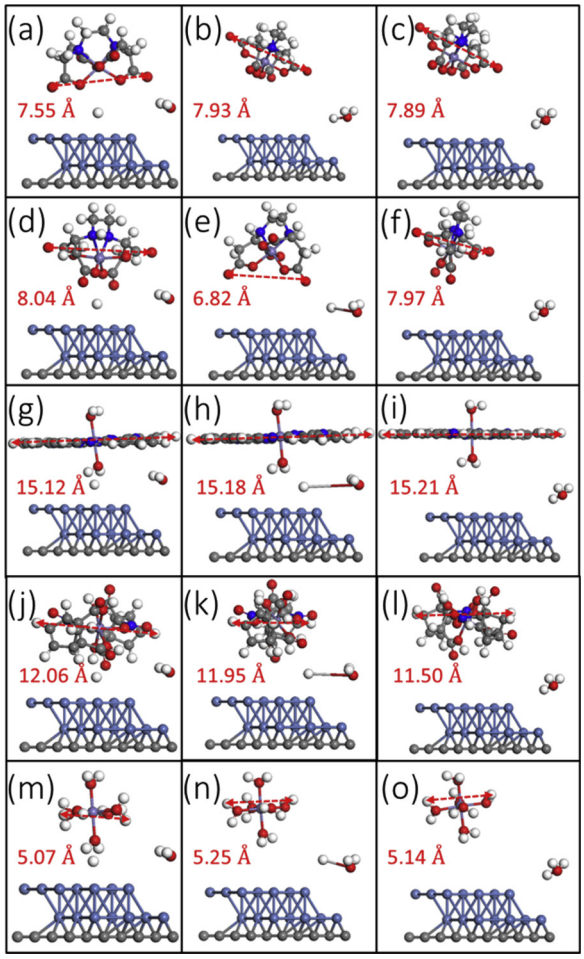

Fig. 8. Optimized structures of atomic H*-dominated $[Fe(III)\text{-}EDTA]^{-}$, $[Fe(III)\text{-}EDDS]^{-}$, $[Fe(III)\text{-}Pc]^{+}\cdot 2H_2O$, $[Fe(III)\text{-}HA]^{3+}$, and $[Fe(H_2O)_6]^{3+}$ reduction on the Ni-CF surface. (a, d, g, j, m): Fe(III)-L, atomic H*, and H_2O, (b, e, h, k, n): transition states, (c, f, i, l, o): Fe(II)-L and H_3O^{+}.

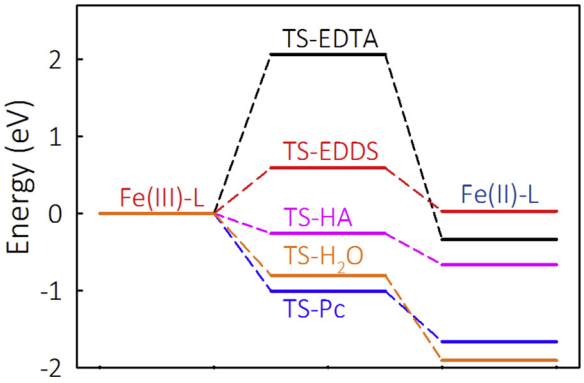

Fig. 9. Energy profile of atomic H*-dominated Fe(III)-L reduction on the Ni-CF surface. The values in the middle and right are the activation energies and reaction energies, respectively.

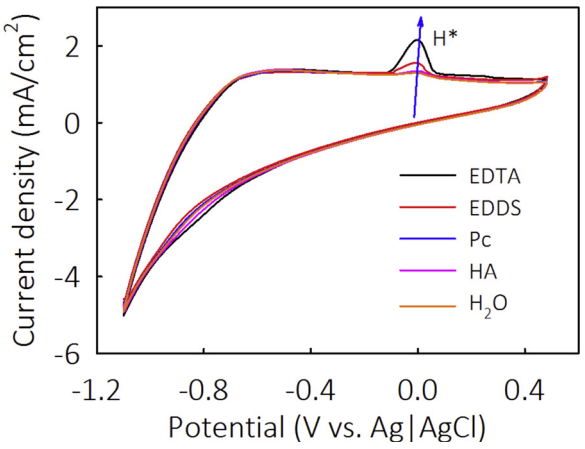

Fig. 10. CV curves in the presence of $[Fe(III)\text{-}EDTA]^-$, $[Fe(III)\text{-}EDDS]^-$, $[Fe(III)\text{-}Pc]^+\cdot 2H_2O$, $[Fe(III)\text{-}HA]^{3+}$, and $[Fe(H_2O)_6]^{3+}$ with Ni-CF at neutral pH.

would have the limited effect on Fe(III) reduction during the EF process, it might deserve a further investigation for the specific ligand to reach convincing conclusions.

As compared to the positive aspects, the produced hydroxyl radicals may affect the cathodic Fe(III) reduction and Fe(II) regeneration in the following two manners. On one hand, Fe(II)-L could be oxidized into Fe(III)-L by hydroxyl radicals to slow down the Fe(III) reduction [49]. On the other hand, the hydroxyl radicals could also degrade ligands in aqueous solution by eliminating the dissolved Fe species, contributing to the generation of solid $Fe(OH)_3$/ferrihydrite with adsorbed Fe(III) [7,36]. The Fe(III) on the surface of $Fe(OH)_3$/ferrihydrite would be reduced into adsorbed Fe(II) by H_2O_2 [51], which mainly occur in the lack of efficient chelating agent. Indeed, the heterogeneous Fenton inspired by adsorbed Fe(II) reduction would occur at neutral pH with Fe^{2+} in the absence of chelator [53,54], but seems to lead to much low pollutant degradation in this study (Fig. 1a and b). This process could be an efficient degradation pathway with rational catalyst design [55–57].

In order to study the effect of iron precipitation during this process, the ICP analysis was conducted to quantify the dissolved iron before and after degradation process. As shown in Fig S5, the insoluble iron contents in the presence of EDTA (2.34 mg/L), EDDS (4.12 mg/L), and HA (2.20 mg/L) were lower than that of Pc (9.47 mg/L) after degradation with the CF cathode. Even the highest concentration of 9.47 mg/L Fe (equivalent to 16.27 mg/L $5Fe_2O_3{\cdot}9H_2O$ or 18.09 mg/L Fe $(OH)_3$), the insoluble iron content was still much lower than one fiftieth of the commonly used catalyst concentration in the heterogeneous Fenton process, such as ca. 1 g/L [53]. Moreover, the heterogeneous Fenton degradation efficiency of $Fe(OH)_3$/ferrihydrite is known to be poor without modification [53]. Hence, the Fe(III) reduction on the surface of iron precipitation was likely much limited as compared to cathodic reduction in this study, which could be confirmed by the IBU degradation with H_2O_2 addition (Fig. S4).

4. Conclusions

This study demonstrates that the properties of iron chelates are vital for their reduction in a neutral EF process. Electron reduction occurs more readily in Fe(III) chelates with LUMO distribution concentrated around the Fe atom and low $E_{LUMO\text{-}HOMO}$. In the electron-dominated EF system, the low $E_{LUMO\text{-}HOMO}$ for $[Fe(III)\text{-}EDTA]^-$ and [Fe(III)-EDDS]- leads to 16.23 and 8.31 times higher degradation rate than that without the addition of the ligand. The atomic H* facilitated the reduction of several Fe(III)-chelates with negative energy barriers and the reduction occurred more readily in systems with high chelation efficiency, such as 10 times faster of $[Fe(III)\text{-}HA]^{3+}$ reduction in atomic H*-dominated system than electron-dominated one. In the lack of efficient chelate, the atomic H*-dominated EF system could also achieve 3 times faster degradation rate than electron-dominated EF system due to the negative energy barrier for the atomic H* reduction of $[Fe(H_2O)_6]^{3+}$. The reduction of Fe(III) chelates is of great significance to the neutral EF process, and the results of this study provided a deep understanding of Fe(III) chelates, their reduction priority, as well as their effects on degrading pollutants in EF systems. The results of this study indicated that pollutant degradation in the neutral EF process was correlated with the chelate structure and the cathode-introduced reductive species. Therefore, researchers should carefully consider the coupling effect between the chelate properties and the dominant reductive species before implementing the EF process for pollutant degradation. Moreover, our findings could also be extended to other Fenton-related processes involved in the interaction between Fe(III) chelates and reductive species, such as H_2O_2, organic radicals ($R^{\cdot}$), $HO_2^{\cdot}$, and $O_2^{\cdot-}$.

CRediT authorship contribution statement

Xiao-Cheng Liu: Methodology, Data curation, Writing - original draft. **Chuan-Shu He:** Data curation, Software, Writing - review & editing. **Zi-Yang Shen:** Software, Validation. **Wen-Qiang Li:** Investigation, Validation. **Ning Chen:** Methodology, Data curation. **Jun-Sheng Song:** Investigation. **Xiao-Guo Zhou:** Investigation. **Yang**

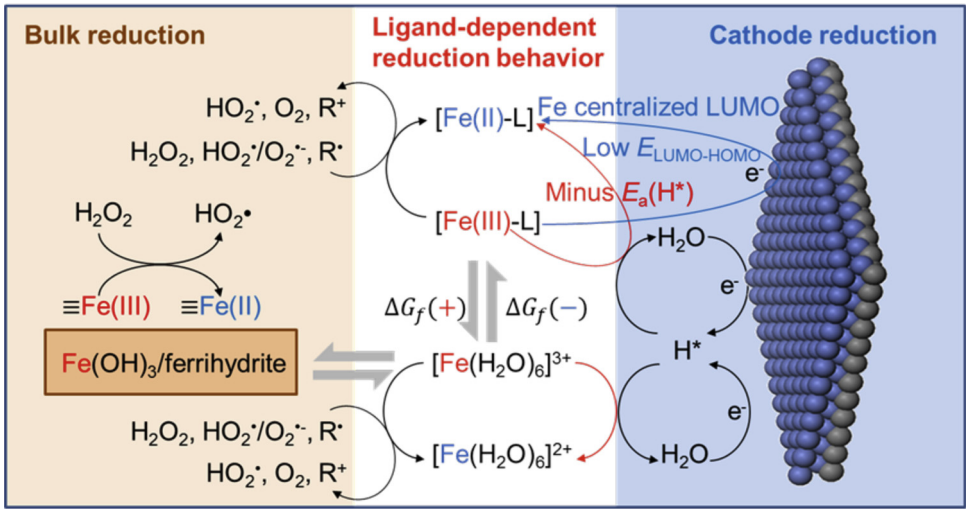

Scheme 1. Possible bulk and cathode reduction mechanism of Fe(III) in neutral EF process.

Mu: Data curation, Writing - review & editing, Supervision, Funding acquisition.

Declaration of Competing Interest

The authors declare that they have no known competing financial interests or personal relationships that could have appeared to influence the work reported in this paper.

Acknowledgements

The authors wish to thank the National Natural Science Foundation of China (U19A20108, 51538012, 51821006, and 51878637) for financially supporting this study. Supercomputing center of USTC is acknowledged for computational support.

Appendix A. Supplementary data

Supplementary material related to this article can be found, in the online version, at doi:https://doi.org/10.1016/j.apcatb.2020.119347.

References

[1] X. Liu, Y. Zhou, J. Zhang, L. Luo, Y. Yang, H. Huang, H. Peng, L. Tang, Y. Mu, Insight into electro-Fenton and photo-Fenton for the degradation of antibiotics: mechanism study and research gaps, Chem. Eng. J. 347 (2018) 379–397, https://doi.org/10.1016/j.cej.2018.04.142.
[2] Y. Zhang, M. Zhou, A critical review of the application of chelating agents to enable Fenton and Fenton-like reactions at high pH values, J. Hazard. Mater. 362 (2019) 436–450, https://doi.org/10.1016/j.jhazmat.2018.09.035.
[3] L. Clarizia, D. Russo, I. Di Somma, R. Marotta, R. Andreozzi, Homogeneous photo-Fenton processes at near neutral pH: a review, Appl. Catal. B: Environ. 209 (2017) 358–371, https://doi.org/10.1016/j.apcatb.2017.03.011.
[4] E. Brillas, I. Sirés, M.A. Oturan, Electro-Fenton process and related electrochemical technologies based on Fenton's reaction chemistry, Chem. Rev. 109 (2009) 6570–6631, https://doi.org/10.1021/cr900136g.
[5] H. He, Z. Zhou, Electro-Fenton process for water and wastewater treatment, Crit. Rev. Environ. Sci. Technol. 47 (2017) 2100–2131, https://doi.org/10.1080/10643389.2017.1405673.
[6] W. Li, C. Menghua, A. Zhihui, Z. Lizhi, Design of a highly efficient and wide pH electro-Fenton oxidation system with molecular oxygen activated by ferrous-tetrapolyphosphate complex, Environ. Sci. Technol. 49 (2015) 3032–3039, https://doi.org/10.1021/es505984y.
[7] Z. Ye, E. Brillas, F. Centellas, P.L. Cabot, I. Sirés, Electro-Fenton process at mild pH using Fe (III)-EDDS as soluble catalyst and carbon felt as cathode, Appl. Catal. B: Environ. 257 (2019) 117907, https://doi.org/10.1016/j.apcatb.2019.117907.
[8] Z. Zhu, Y. Chen, Y. Gu, F. Wu, W. Lu, T. Xu, W. Chen, Catalytic degradation of recalcitrant pollutants by Fenton-like process using polyacrylonitrile-supported iron (II) phthalocyanine nanofibers: intermediates and pathway, Water Res. 93 (2016) 296–305, https://doi.org/10.1016/j.watres.2016.02.035.
[9] C. He, D. He, R.N. Collins, S. Garg, Y. Mu, T.D. Waite, Effects of good's buffers and pH on the structural transformation of zero valent Iron and the oxidative degradation of contaminants, Environ. Sci. Technol. 52 (2018) 1393–1403, https://doi.org/10.1021/acs.est.7b04030.
[10] X.-C. Liu, W.-Q. Li, Y.-R. Wang, G.-N. Zhou, Y.-X. Wang, C.-S. He, G.-M. Wang, Y. Mu, Cathode-introduced atomic H* for Fe (II)-Complex regeneration to effective electro-Fenton process at a natural pH, Environ. Sci. Technol. 53 (2019) 6927–6936, https://doi.org/10.1021/acs.est.9b00345.
[11] O.R. Brown, S.A. Thornton, Kinetics of electrode reactions in liquid ammonia. Part 2.—Fe^{III}/Fe^{II} and Co^{III}/Co^{II} redox couples, J. Chem. Soc. Faraday T. 70 (1974) 14–26, https://doi.org/10.1039/f19747000014.
[12] G. Chauhan, M. Stein, A. Seidel-Morgenstern, K.K. Pant, K.D. Nigam, The thermodynamics and biodegradability of chelating agents upon metal extraction, Chem. Eng. Sci. 137 (2015) 768–785, https://doi.org/10.1016/j.ces.2015.07.028.
[13] M.D. Kuz'min, R. Hayn, V. Oison, Ab initio calculated XANES and XMCD spectra of Fe (II) phthalocyanine, Phys. Rev. B 79 (2009) 024413, https://doi.org/10.1103/PhysRevB.79.024413.
[14] J. Strouse, S.W. Layten, C.E. Strouse, Structural studies of transition metal complexes of triionized and tetraionized citrate. Models for the coordination of the citrate ion to transition metal ions in solution and at the active site of aconitase, J. Am. Chem. Soc. 99 (1977) 562–572, https://doi.org/10.1021/ja00444a041.
[15] E.E. Daugherty, B. Gilbert, P.S. Nico, T. Borch, Complexation and redox buffering of iron (II) by dissolved organic matter, Environ. Sci. Technol. 51 (2017) 11096–11104, https://doi.org/10.1021/acs.est.7b03152.
[16] C.C. Wagner, E.J. Baran, Vibrational spectra of two Fe(III)/EDTA complexes useful for iron supplementation, Spectrochim. Acta A. 75 (2010) 807–810, https://doi.org/10.1016/j.saa.2009.11.059.
[17] R. Alam, T. Mistri, P. Mondal, D. Das, S.K. Mandal, A.R. Khuda-Bukhsh, M. Ali, A novel copper (II) complex as a nitric oxide turn-on fluorosensor: intracellular applications and DFT calculation, Dalton Trans. 43 (2014) 2566–2576, https://doi.org/10.1039/c3dt52521j.
[18] S. Guo, L. Zhu, T. Majima, M. Lei, H. Tang, Reductive debromination of polybrominated diphenyl ethers: dependence on Br number of the Br-Rich phenyl ring, Environ. Sci. Technol. 53 (2019) 4433–4439, https://doi.org/10.1021/acs.est.8b07050.
[19] S. Luo, Z. Wei, R. Spinney, Z. Zhang, D.D. Dionysiou, L. Gao, L. Chai, D. Wang, R. Xiao, UV direct photolysis of sulfamethoxazole and ibuprofen: an experimental and modelling study, J. Hazard. Mater. 343 (2018) 132–139, https://doi.org/10.1016/j.jhazmat.2017.09.019.
[20] P.L. Holland, Electronic structure and reactivity of three-coordinate iron complexes, Acc. Chem. Res. 41 (2008) 905–914, https://doi.org/10.1021/ar700267b.
[21] A. Liu, R.D. Gonzalez, Modeling adsorption of copper (II), cadmium (II) and lead (II) on purified humic acid, Langmuir 16 (2000) 3902–3909, https://doi.org/10.1021/la990607x.
[22] F. Mendez-Arriaga, S. Esplugas, J. Gimenez, Degradation of the emerging contaminant ibuprofen in water by photo-Fenton, Water Res. 44 (2010) 589–595, https://doi.org/10.1016/j.watres.2009.07.009.
[23] L. Xing, N. Chen, W. Fan, M. Li, X. Zhou, S. Liu, Double-edged effects of aluminium ions on amyloid fibrillation of hen egg-white lysozyme, Int. J. Biol. Macromol. 132 (2019) 929–938, https://doi.org/10.1016/j.ijbiomac.2019.04.009.
[24] L. Xing, W. Fan, N. Chen, M. Li, X. Zhou, S. Liu, Amyloid formation kinetics of hen egg white lysozyme under heat and acidic conditions revealed by Raman spectroscopy, J. Raman Spectrosc. (2019), https://doi.org/10.1002/jrs.5567.
[25] J.-J. Chen, W. Chen, H. He, D.-B. Li, W.-W. Li, L. Xiong, H.-Q. Yu, Manipulation of microbial extracellular electron transfer by changing molecular structure of phenazine-type redox mediators, Environ. Sci. Technol. 47 (2012) 1033–1039, https://doi.org/10.1021/es304189t.
[26] L. Gong, J.-J. Chen, Y. Mu, Catalytic CO_2 reduction to valuable chemicals using NiFe-based nanoclusters: a first-principles theoretical evaluation, Phys. Chem. Chem. Phys. 19 (2017) 28344–28353, https://doi.org/10.1039/C7CP06155B.
[27] M. Sun, A.E. Nelson, J. Adjaye, Adsorption thermodynamics of sulfur-and nitrogen-containing molecules on NiMoS: a DFT study, Catal. Lett. 109 (2006) 133–138, https://doi.org/10.1007/s10562-006-0069-z.
[28] C. Bressler, C. Milne, V.-T. Pham, A. ElNahhas, R.M. van der Veen, W. Gawelda, S. Johnson, P. Beaud, D. Grolimund, M. Kaiser, Femtosecond XANES study of the light-induced spin crossover dynamics in an iron (II) complex, Science 323 (2009) 489–492, https://doi.org/10.1126/science.1165733.
[29] D. Harris, G.H. Loew, A. Komornicki, Structure and relative spin-state energetics of $[Fe(H_2O)_6]^{3+}$: a comparison of UHF, møller−Plesset, nonlocal DFT, and semi-empircal INDO/S calculations, J. Phys. Chem. A 101 (1997) 3959–3965 https://doi.org/.1021/jp963296x.
[30] A. Hauser, C. Enachescu, M.L. Daku, A. Vargas, N. Amstutz, Low-temperature lifetimes of metastable high-spin states in spin-crossover and in low-spin iron (II) compounds: The rule and exceptions to the rule, Coord. Chem. Rev. 250 (2006) 1642–1652, https://doi.org/10.1016/j.ccr.2005.12.006.
[31] Y. Lei, B. Song, R.D. van der Weijden, M. Saakes, C.J.N. Buisman, Electrochemical induced calcium phosphate precipitation: importance of local pH, Environ. Sci. Technol. 51 (2017) 11156–11164, https://doi.org/10.1021/acs.est.7b03909.
[32] M. Skoumal, R.M. Rodríguez, P.L. Cabot, F. Centellas, J.A. Garrido, C. Arias, E. Brillas, Electro-Fenton, UVA photoelectro-Fenton and solar photoelectro-Fenton degradation of the drug ibuprofen in acid aqueous medium using platinum and boron-doped diamond anodes, Electrochim. Acta 54 (2009) 2077–2085, https://doi.org/10.1016/j.electacta.2008.07.014.
[33] K. Dot, Thermometric studies on the Fe(III)—EDTA chelate, Talanta 25 (1978) 97–101, https://doi.org/10.1016/0039-9140(78)80040-X.
[34] F.C. Moreira, R.A.R. Boaventura, E. Brillas, V.J.P. Vilar, Electrochemical advanced oxidation processes: a review on their application to synthetic and real wastewaters, Appl. Catal. B: Environ. 202 (2017) 217–261, https://doi.org/10.1016/j.apcatb.2016.08.037.
[35] C. Jiang, S. Garg, T.D. Waite, Hydroquinone-mediated redox cycling of Iron and concomitant oxidation of hydroquinone in oxic waters under acidic conditions: comparison with Iron–natural organic matter interactions, Environ. Sci. Technol. 49 (2015) 14076–14084, https://doi.org/10.1021/acs.est.5b03189.
[36] Z. Ye, E. Brillas, F. Centellas, P.L. Cabot, I. Sirés, Expanding the application of photoelectro-Fenton treatment to urban wastewater using the Fe(III)-EDDS complex, Water Res. 169 (2020) 115219, https://doi.org/10.1016/j.watres.2019.115219.
[37] N. Walker, J. Mintz, Hydrolysis of the carbonate ion, J. Chem. Educ. 47 (1970) A119, https://doi.org/10.1021/ed047pA119.1.
[38] S. Haraguchi, T. Shingae, T. Fujisawa, N. Kasai, M. Kumauchi, T. Hanamoto, W.D. Hoff, M. Unno, Spectroscopic ruler for measuring active-site distortions based on Raman optical activity of a hydrogen out-of-plane vibration, Proc. Natl. Acad. Sci. U. S. A. 115 (2018) 8671–8675, https://doi.org/10.1073/pnas.1806491115.
[39] M.H.V. Huynh, T.J. Meyer, Proton-coupled electron transfer, Chem. Rev. 107 (2007) 5004–5064, https://doi.org/10.1039/9781849733168.
[40] Z. Chen, Y. Song, J. Cai, X. Zheng, D. Han, Y. Wu, Y. Zang, S. Niu, Y. Liu, J. Zhu, X. Liu, G. Wang, Tailoring the d-Band centers enables Co_4N nanosheets to be highly active for hydrogen evolution catalysis, Angew. Chem., Int. Ed. 57 (2018) 5076–5080, https://doi.org/10.1002/ange.201801834.
[41] C. Spike, R. Parry, Thermodynamics of chelation. II. Bond energy effects in chelate ring formation, J. Am. Chem. Soc. 75 (1953) 3770–3772, https://doi.org/10.1021/ja01111a049.
[42] M. Lee, S.G. Zimmermann-Steffens, J.S. Arey, K. Fenner, U. von Gunten, Development of prediction models for the reactivity of organic compounds with

ozone in aqueous solution by quantum chemical calculations: the role of delocalized and localized molecular orbitals, Environ. Sci. Technol. 49 (2015) 9925–9935, https://doi.org/10.1021/acs.est.5b00902.
[43] Y.-S. Keum, Q.X. Li, Reductive debromination of polybrominated diphenyl ethers by zerovalent iron, Environ. Sci. Technol. 39 (2005) 2280–2286, https://doi.org/10.1021/es048846g.
[44] M.P. DeMatteo, J.S. Poole, X. Shi, R. Sachdeva, P.G. Hatcher, C.M. Hadad, M.S. Platz, On the electrophilicity of hydroxyl radical: A laser flash photolysis and computational study, J. Am. Chem. Soc. 127 (2005) 7094–7109, https://doi.org/10.1021/ja043692q.
[45] S. Luo, L. Gao, Z. Wei, R. Spinney, D.D. Dionysiou, W.-P. Hu, L. Chai, R. Xiao, Kinetic and mechanistic aspects of hydroxyl radical–mediated degradation of naproxen and reaction intermediates, Water Res. 137 (2018) 233–241, https://doi.org/10.1016/j.watres.2018.03.002.
[46] P. Comba, M. Kerscher, G.A. Lawrance, B. Martin, H. Wadepohl, S. Wunderlich, Stable five-and six-coordinate cobalt (III) complexes with a Pentadentate bispidine ligand, Angew. Chem., Int. Ed. 47 (2008) 4740–4743, https://doi.org/10.1002/anie.200800515.
[47] J.R. Alvarez-Idaboy, N. Mora-Diez, A. Vivier-Bunge, A quantum chemical and classical transition state theory explanation of negative activation energies in OH addition to substituted ethenes, J. Am. Chem. Soc. 122 (2000) 3715–3720, https://doi.org/10.1021/ja993693w.
[48] M. Xing, W. Xu, C. Dong, Y. Bai, J. Zeng, Y. Zhou, J. Zhang, Y. Yin, Metal sulfides as excellent co-catalysts for H_2O_2 decomposition in advanced oxidation processes, Chem 4 (2018) 1359–1372, https://doi.org/10.1016/j.chempr.2018.03.002.
[49] W. Huang, M. Brigante, F. Wu, C. Mousty, K. Hanna, G. Mailhot, Assessment of the Fe (III)–EDDS complex in Fenton-like processes: from the radical formation to the degradation of bisphenol A, Environ. Sci. Technol. 47 (2013) 1952–1959, https://doi.org/10.1021/es304502y.
[50] J.J. Pignatello, E. Oliveros, A. MacKay, Advanced oxidation processes for organic contaminant destruction based on the Fenton reaction and related chemistry, Crit. Rev. Environ. Sci. Technol. 36 (2006) 1–84, https://doi.org/10.1080/10643380500326564.
[51] Y. Zhu, R. Zhu, Y. Xi, J. Zhu, G. Zhu, H. He, Strategies for enhancing the heterogeneous Fenton catalytic reactivity: a review, Appl. Catal. B: Environ. 255 (2019) 117739, https://doi.org/10.1016/j.apcatb.2019.05.041.
[52] F. Gozzo, Radical and non-radical chemistry of the Fenton-like systems in the presence of organic substrates, J. Mol. Catal. A Chem. 171 (2001) 1–22, https://doi.org/10.1016/S1381-1169(01)00099-1.
[53] R. Zhu, Y. Zhu, H. Xian, L. Yan, H. Fu, G. Zhu, Y. Xi, J. Zhu, H. He, CNTs/ferrihydrite as a highly efficient heterogeneous Fenton catalyst for the degradation of bisphenol A: the important role of CNTs in accelerating Fe(III)/Fe(II) cycling, Appl. Catal. B: Environ. 270 (2020) 118891, https://doi.org/10.1016/j.apcatb.2020.118891.
[54] T. Xu, R. Zhu, H. Shang, Y. Xia, X. Liu, L. Zhang, Photochemical behavior of ferrihydrite-oxalate system: interfacial reaction mechanism and charge transfer process, Water Res. 159 (2019) 10–19, https://doi.org/10.1016/j.watres.2019.04.055.
[55] Y. Zhu, R. Zhu, L. Yan, H. Fu, Y. Xi, H. Zhou, G. Zhu, J. Zhu, H. He, Visible-light Ag/AgBr/ferrihydrite catalyst with enhanced heterogeneous photo-Fenton reactivity via electron transfer from Ag/AgBr to ferrihydrite, Appl. Catal. B: Environ. 239 (2018) 280–289, https://doi.org/10.1016/j.apcatb.2018.08.025.
[56] T. Xu, R. Zhu, G. Zhu, J. Zhu, X. Liang, Y. Zhu, H. He, Mechanisms for the enhanced photo-Fenton activity of ferrihydrite modified with $BiVO_4$ at neutral pH, Appl. Catal. B: Environ. 212 (2017) 50–58, https://doi.org/10.1016/j.apcatb.2017.04.064.
[57] Y. Zhong, X. Liang, Z. He, W. Tan, J. Zhu, P. Yuan, R. Zhu, H. He, The constraints of transition metal substitutions (Ti, Cr, Mn, Co and Ni) in magnetite on its catalytic activity in heterogeneous Fenton and UV/Fenton reaction: From the perspective of hydroxyl radical generation, Appl. Catal. B: Environ. 150-151 (2014) 612–618, https://doi.org/10.1016/j.apcatb.2014.01.007.